Computational Investigation of the Effect of Chemistry on Mars Supersonic Retropropulsion Environments

Gabriel Nastac[1], Ashley Korzun[1], Aaron Walden[1], Eric Nielsen[1], William Jones[1], Patrick Moran[2]

[1]NASA Langley Research Center

Hampton, Virginia, 23681

[2]NASA Ames Research Center

Moffett Field, California, 94035

This research used resources of the Oak Ridge Leadership Computing Facility at the Oak Ridge National Laboratory, which is supported by the Office of Science of the U.S. Department of Energy under Contract No. DE-AC05-00OR22725.

Retropropulsion for Human Mars Exploration

Human-scale Mars landers require new approaches to all phases of Entry, Descent, and Landing

- Cannot use heritage, low-L/D rigid capsules → deployable hypersonic decelerators or mid-L/D rigid aeroshells
- Cannot use parachutes → retropropulsion, from supersonic conditions to touchdown
- No viable alternative to an extended, retropropulsive phase of flight

	Viking	Pathfinder	MERs	Phoenix	MSL	InSight	M2020	Human-Scale Lander (Projected)
Entry Capsule (to scale)								
Diameter (m)	3.505	2.65	2.65	2.65	4.52	2.65	4.5	16 - 19
Entry Mass (t)	0.930	0.584	0.832	0.573	3.153	0.608	3.440	49 - 65
Parachute Diameter (m)	16.0	12.5	14.0	11.8	19.7	11.8	21.5	N/A
Parachute Deploy (Mach)	1.1	1.57	1.77	1.65	1.75	1.66	1.75	N/A
Landed Mass (t)	0.603	0.360	0.539	0.364	0.899	0.375	1.050	26 - 36
Landing Altitude (km)	-3.5	-2.5	-1.4	-4.1	-4.4	-2.6	-2.5	+/- 2.0
Landing Technology	 Retro-propulsion	 Airbags	 Airbags	 Retro-propulsion	 Skycrane	 Retro-propulsion	 Skycrane	Supersonic Retropropulsion

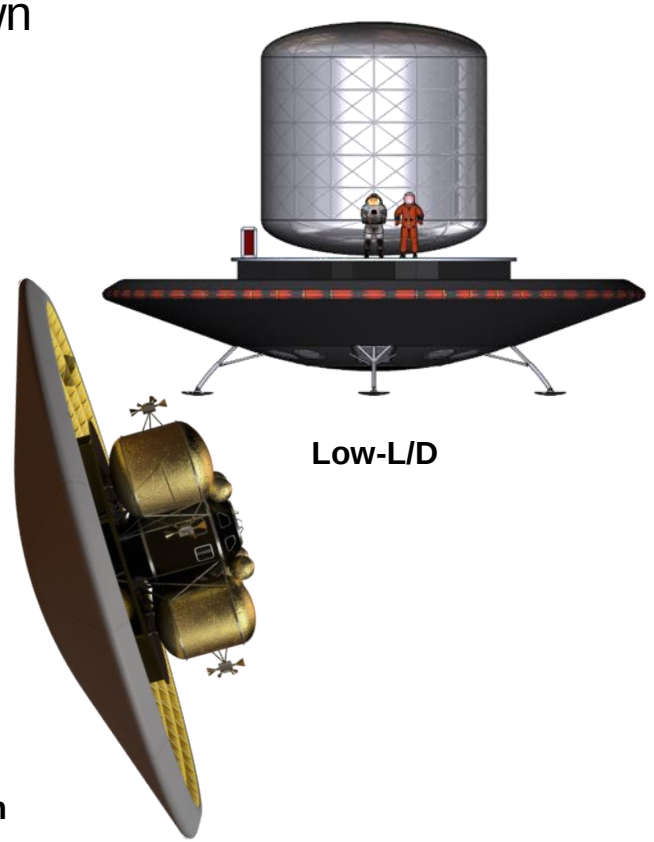

Low-L/D

Steady progression of "in family" EDL

New EDL Paradigm

Motivation

- Retropropulsion ground tests require significant compromises on physical scale, instrumentation, configuration, and environments
- Past simulation work primarily focused on perfect gas flows
- Past work by the authors investigated a Mars lander concept scaled for perfect gas air
- **In this work, we investigate the effects of chemistry using scale-resolved finite-rate chemistry CFD of a Mars lander concept at realistic Martian supersonic conditions. An overview of the broader campaign is presented in an accompanying talk[1]**

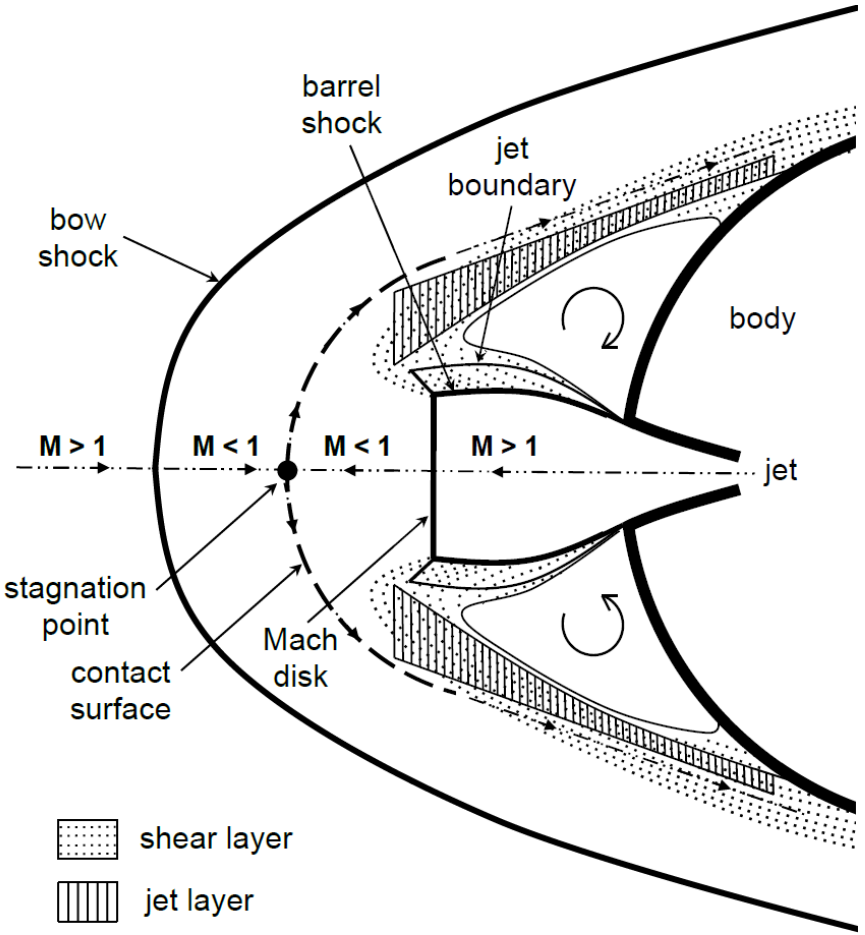

[1]Ashley Korzun, Gabriel Nastac, Aaron Walden, Eric J. Nielsen, William Jones, and Patrick Moran. "Application of a Detached Eddy Simulation Approach with Finite-Rate Chemistry to Mars-Relevant Retropropulsion Operating Environments," AIAA SciTech 2022 Forum. January 2022.

Simulation Overview

- To maintain **dynamic similitude**, various key parameters are matched between the perfect gas and finite-rate chemistry
- **Throttle conditions of 60% and 80% are examined to quantify differences between overexpanded and underexpanded nozzles**
- Incorporation of a 10 species chemical mechanism for the oxygen/methane engines leads to over **an order of magnitude higher computational expense over perfect gas**
- The Summit supercomputer at ORNL is utilized for these runs, enabling full-scale simulations encompassing seconds of physical time in a few days using thousands of GPUs (equivalent to several million CPU cores)
- The GPU implementation[1] employs hierarchical parallelism as well as general GPU optimizations to enable performant and scalable chemistry kernels

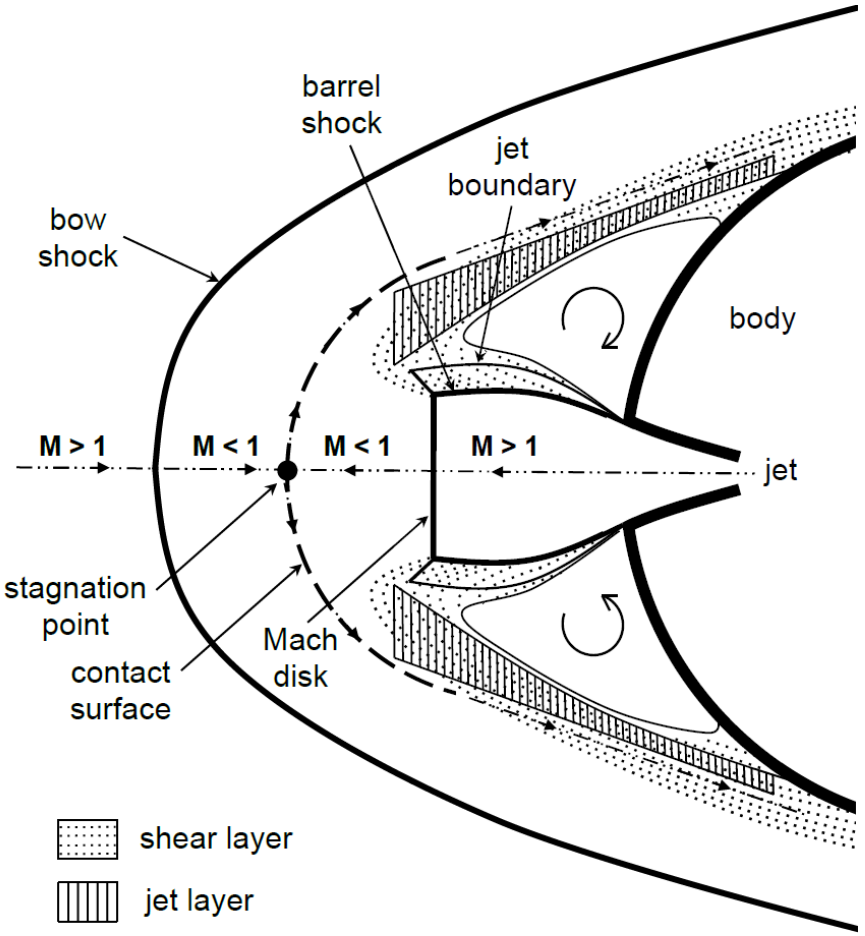

[1]Gabriel Nastac, Aaron Walden, Eric J. Nielsen, and Kader Frendi. "Implicit Thermochemical Nonequilibrium Flow Simulations on Unstructured Grids using GPUs," AIAA 2021-0159. AIAA SciTech 2021 Forum. January 2021.

Governing Equations and Numerical Implementation

- NASA FUN3D is the flow solver used for this work
- Node-based finite-volume approach on general unstructured grids
- Thermochemical Nonequilibrium (“Generic Gas”) path is used
- Conservation of species, momentum, energies, and turbulence variables
- Two-temperature model available for thermal nonequilibrium
- 2 equation models (e.g., SST), Spalart-Allmaras turbulence model with Catris-Aupoix compressibility correction; DES option
- Variable species, energies, and turbulence equations
- Fully implicit formulations are used to integrate the equations in time
  - Sparse block linear system: $A\boldsymbol{x} = \boldsymbol{b}$
  - Matrix A composed of diagonal and off-diagonal $N_{eq}\,x\,N_{eq}$ blocks
  - Memory and solution time increases as $O\left(N_{eq}^2\right)$
- System solved with multicolor point-implicit approach

$$\frac{\partial}{\partial t}(\rho y_s) + \frac{\partial}{\partial x_j}(\rho y_s u_j) - \frac{\partial}{\partial x_j}(J_{sj}) = \dot{\omega}_s$$

$$\frac{\partial}{\partial t}(\rho u_i) + \frac{\partial}{\partial x_j}(\rho u_i u_j + p\delta_{ij}) - \frac{\partial}{\partial x_j}(\tau_{ij}) = 0$$

$$\frac{\partial}{\partial t}(\rho E) + \frac{\partial}{\partial x_j}\left((\rho E + p)u_j\right) - \frac{\partial}{\partial x_j}\left(u_k\tau_{kj} + \dot{q}_j + \sum_{s=1}^{N_s} h_s J_{sj}\right) = 0$$

$$\frac{\partial}{\partial t}(\rho E_v) + \frac{\partial}{\partial x_j}(\rho E_v u_j) - \frac{\partial}{\partial x_j}\left(\dot{q}_{V\,j} + \sum_{s=1}^{N_s} h_{V\,s} J_{sj}\right) = S_v$$

$$\frac{\partial}{\partial t}(\rho\tilde{\nu}) + \frac{\partial}{\partial x_j}(\rho\tilde{\nu}u_j) - \frac{\partial}{\partial x_j}\left(\frac{1}{\sigma}\left(\mu\frac{\partial\tilde{\nu}}{\partial x_j} + \sqrt{\rho}\tilde{\nu}\frac{\partial\sqrt{\rho}\tilde{\nu}}{\partial x_j}\right)\right) = S_{\tilde{\nu}}$$

$$\boldsymbol{q} = [\rho\vec{y}_s, \rho\vec{u}, \rho E, \rho E_v, \rho\tilde{\nu}]^T$$

$$\int_V \frac{\partial \boldsymbol{q}}{\partial t} dV + \oint_S (\boldsymbol{F}\cdot\boldsymbol{n}) dS - \int_V \boldsymbol{S} dV = \boldsymbol{0}$$

$$\left[\frac{V}{\Delta\tau}\boldsymbol{I} + \frac{V}{\Delta t}\boldsymbol{I} + \frac{\partial\widehat{\boldsymbol{R}}}{\partial\boldsymbol{q}}\right]\Delta\mathbf{q} = -\mathbf{R}(\mathbf{q}^{n+1,m}) - \frac{V}{\Delta \mathrm{t}}(\mathbf{q}^{n+1,m} - \mathbf{q}^{\mathrm{n}})$$

$$\mathbf{q}^{n+1,m} = \mathbf{q}^{n+1,m} + \Delta\boldsymbol{q}$$

Supersonic Retropropulsion Flow for a Single Engine Vehicle

- Simulations of previous perfect gas air experimental setup are performed to incorporate SA-Catris DES, focusing on single nozzle runs (Run 165)
- $M_\infty = 4.6,\ Re_\infty = 5 \times 10^6 \frac{1}{m},\ \frac{p_0}{p_\infty} = 7724.3, \frac{T_0}{T_\infty} = 5.34$
- 70-degree sphere cone with $D = 5$ in, with nozzle exit diameter $\Phi = 0.5$ in
- **SA-Catris DES is comparable to SA DES, with slightly improved surface pressure predictions**

Mach Number

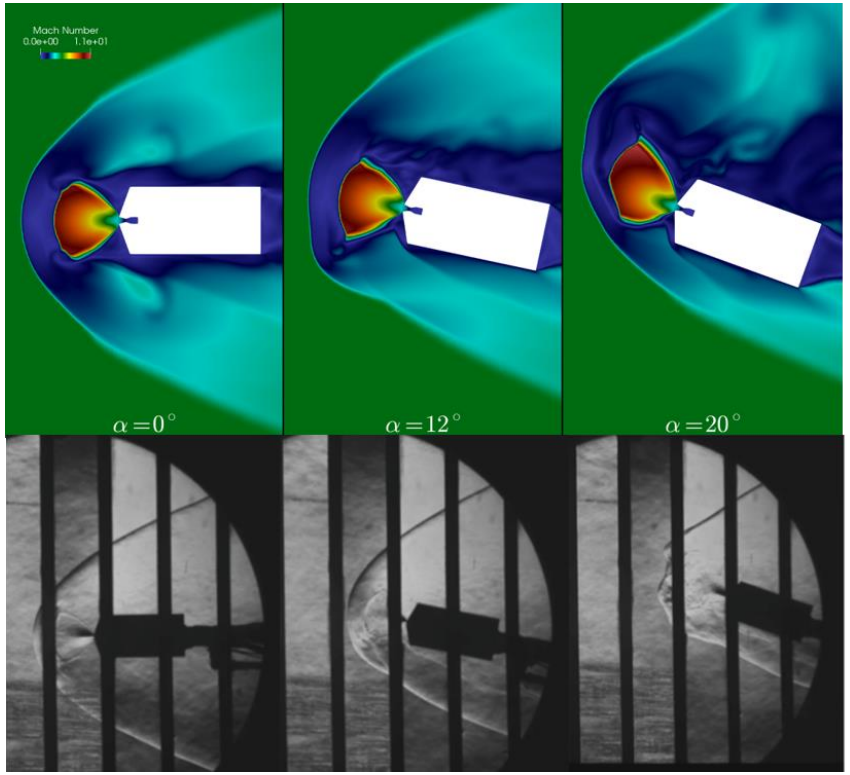

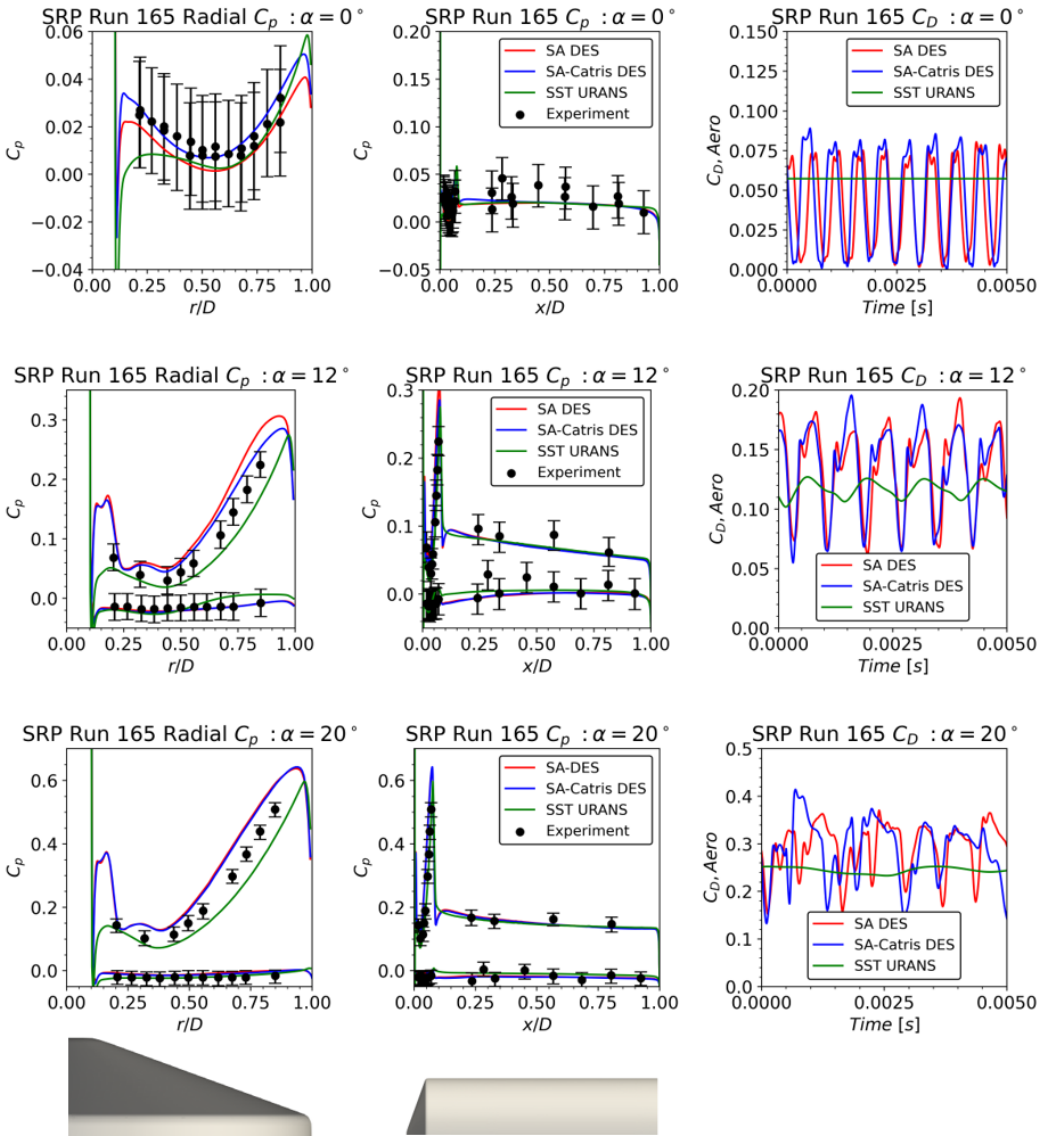

Vehicle and Grid

- Vehicle diameter is nominally 16.4 meters
- 8 identical scarfed engines, $A_e/A_t = 177$
- Coarse grid consists of 139M points
- Fine grid consists of 1.1B points
- Walls are resolved with $y^+ \approx 1$
- Details in paper

Centerline slice of nozzle grid for 139 million point grid

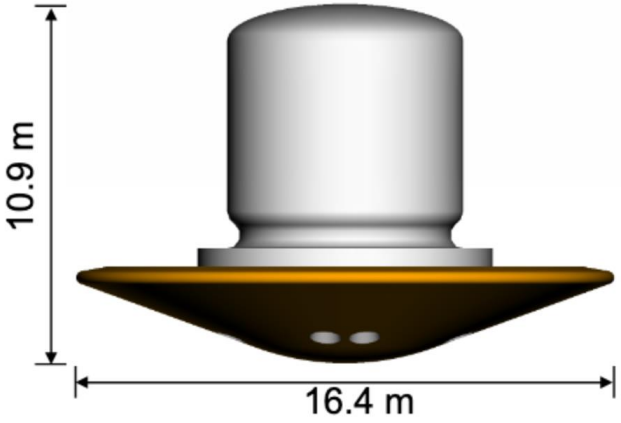

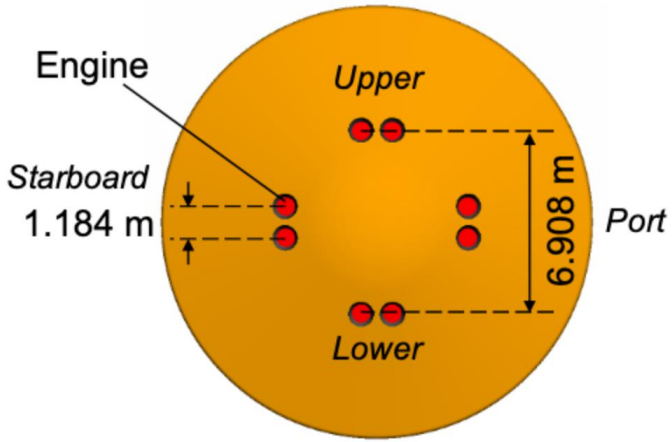

Surface grid for 139 million point grid

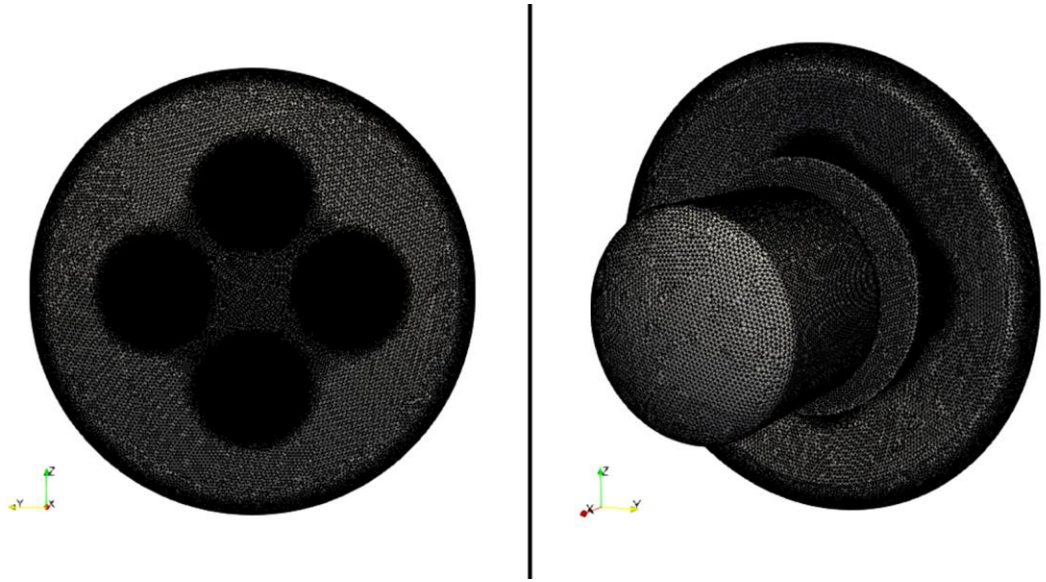

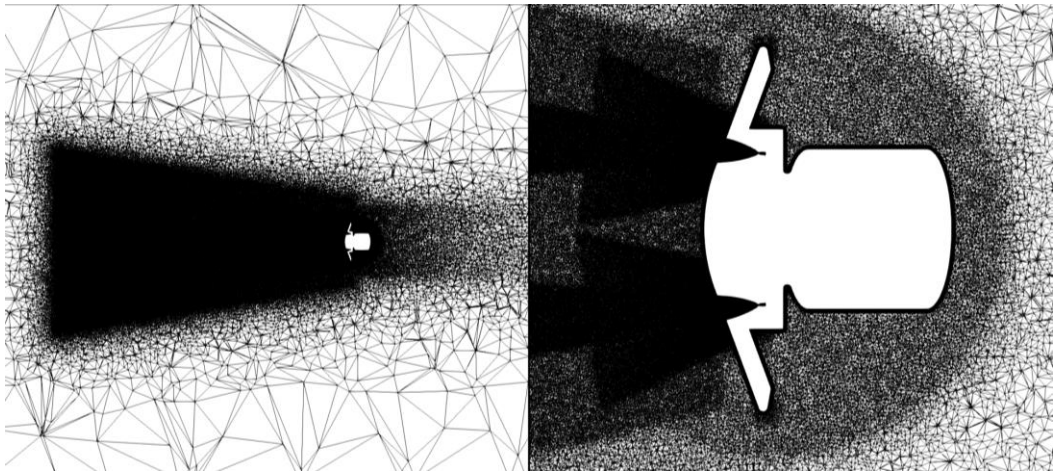

Centerline slice of volume grid for 139 million point grid

Modeling Overview

- $M_\infty = 2.4$, $Re_D \approx 5.9 \times 10^6$
- Martian atmosphere (97% CO_2, 3% N_2 by mass)
- Engine plena set an equilibrium composition of the products of methane-oxygen combustion
  - O/F = 3.5 with $T_0 = 3582$ K
- 10-species, 19-reaction chemical mechanism (detailed in paper)
- Total pressure varies based on throttle:
  - 84.5 bar (80%) and 63.3 bar (60%)
- Walls are modeled as no slip
- The turbulent boundary layer, δ_{99}, at the nozzle exits is approximately 8% of the exit nozzle radius
- Ratio of nozzle lip pressure to pressure outside the nozzles is key for prediction of under- or over-expanded nozzle conditions

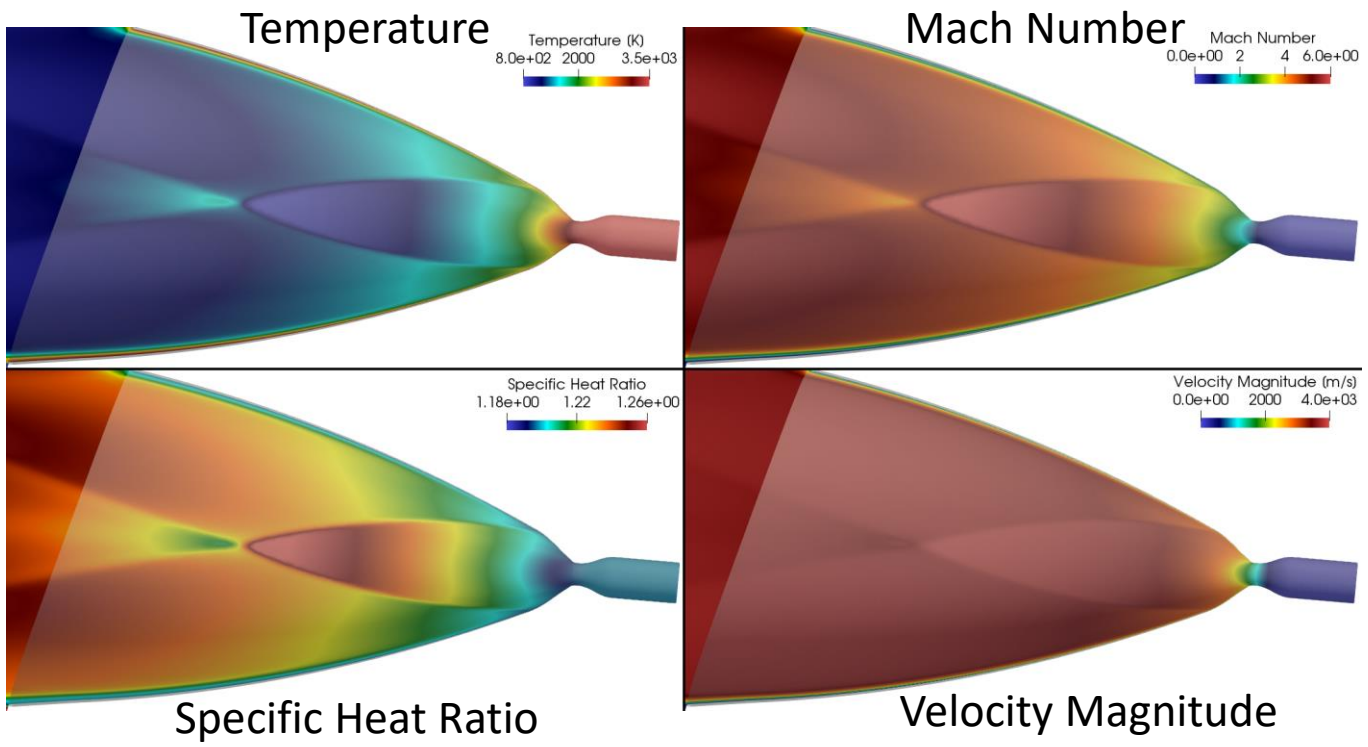

Flowfield Visualization for 80% Throttle (1/3)

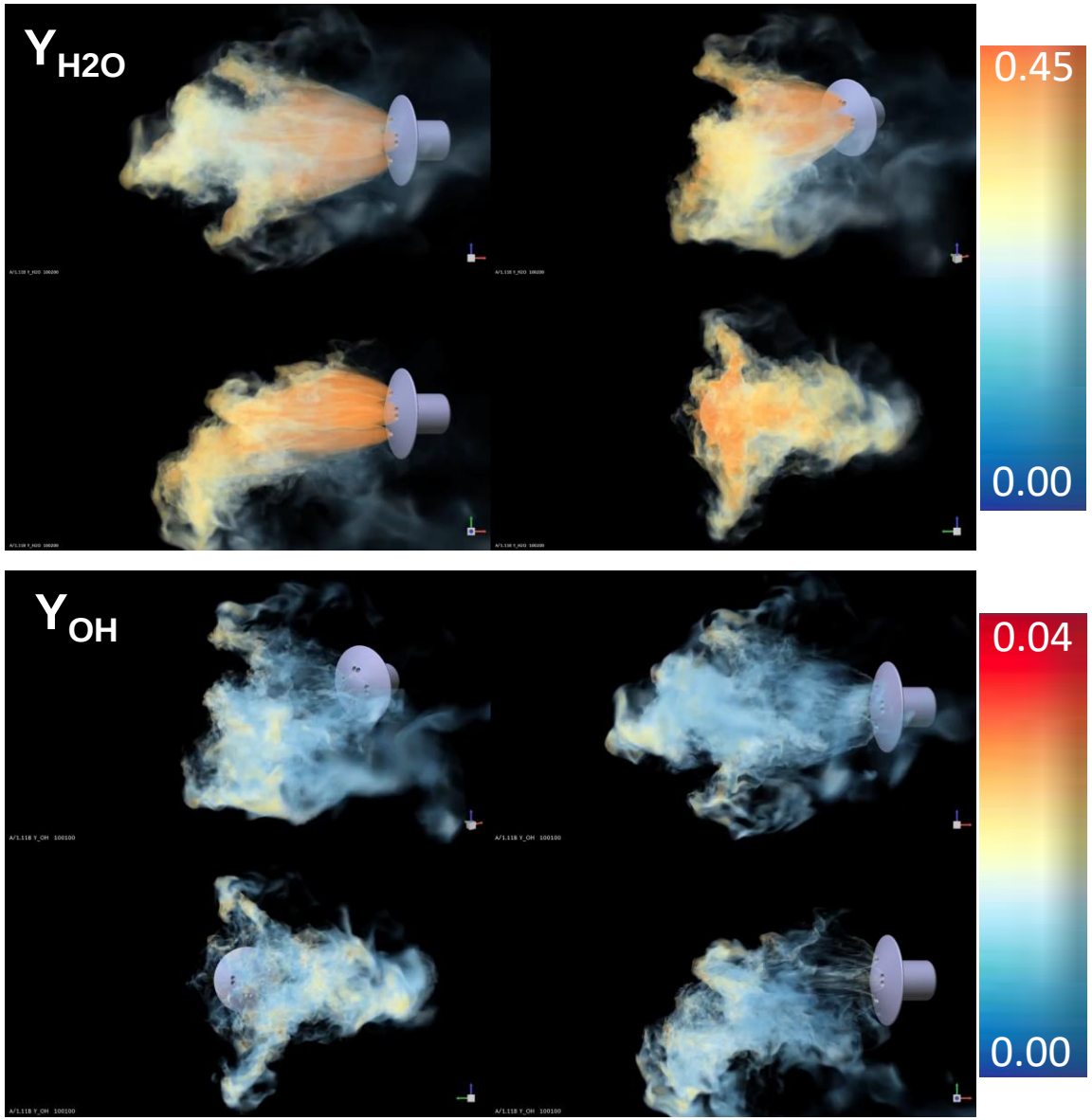

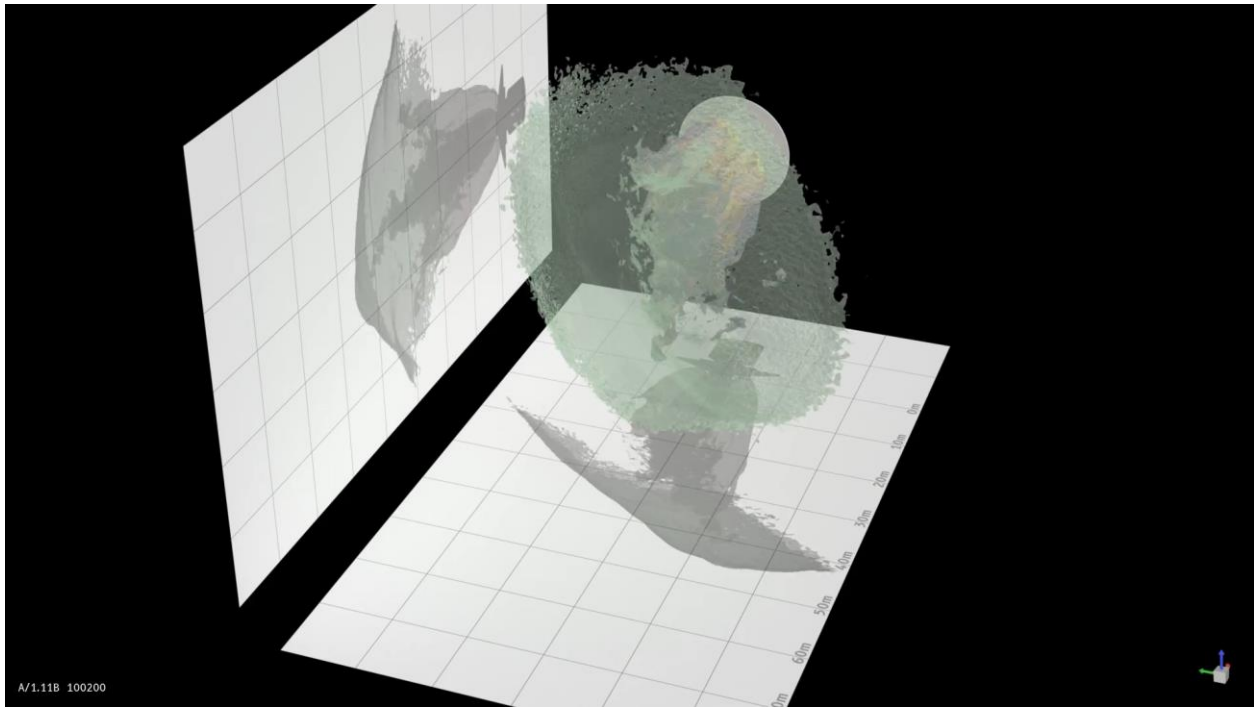

Isosurfaces of Y_{H_2O} (0.4) colored by vorticity magnitude and bow shock
(each Cartesian grid line represents 10 meters)

Flowfield Visualization for 80% Throttle (2/3)

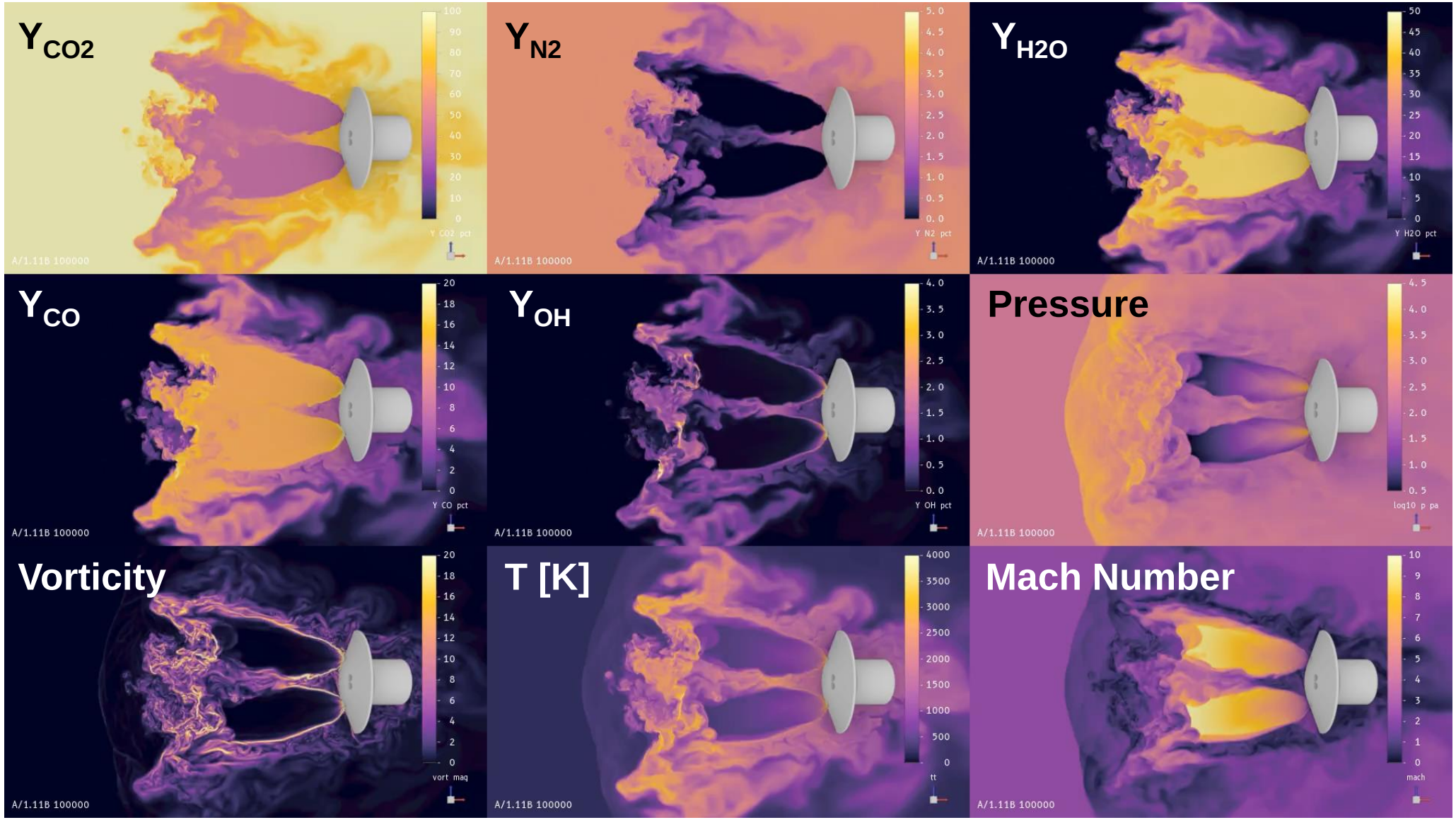

Flowfield Visualization for 80% Throttle (3/3)

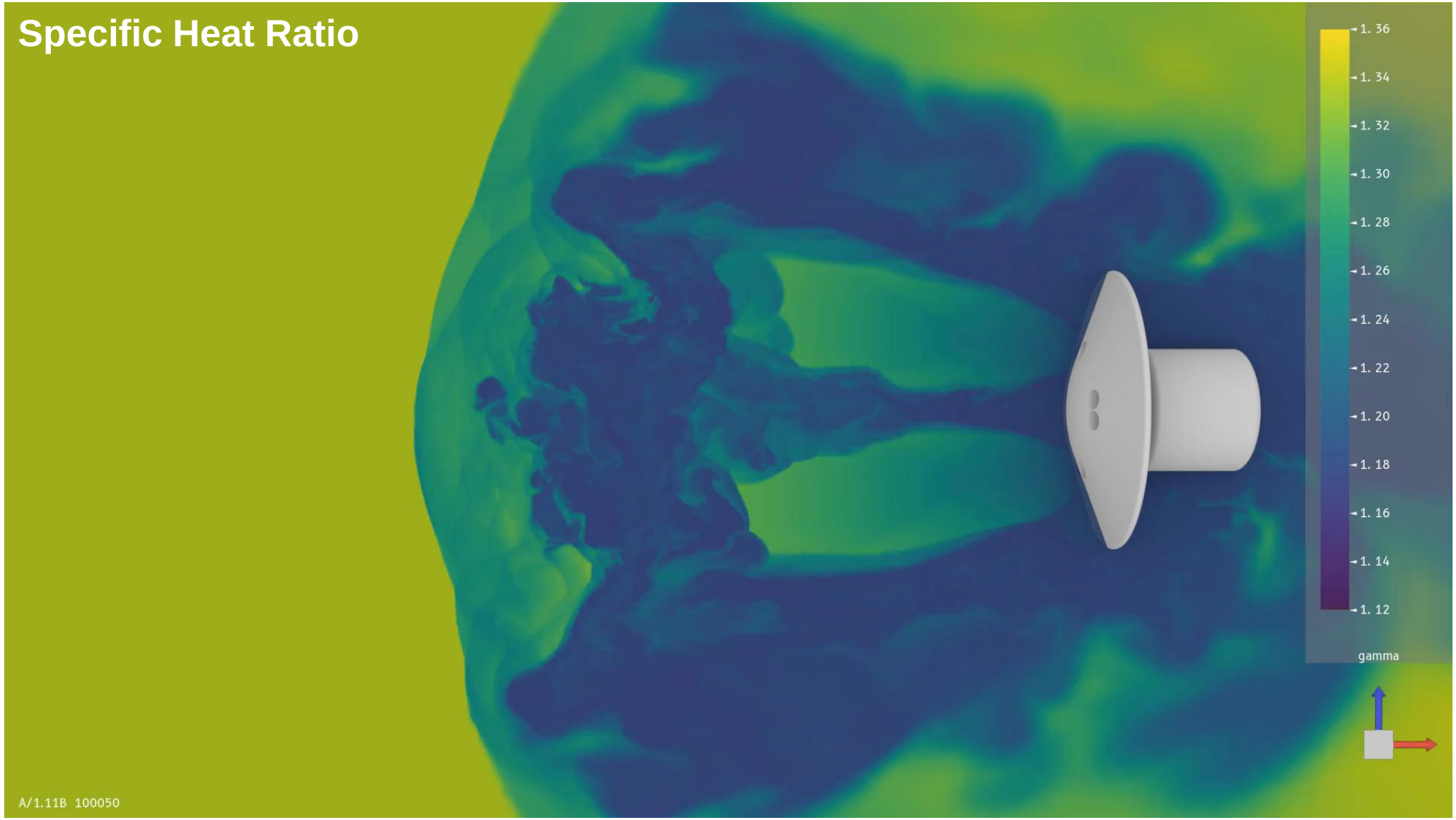

Effect of Throttling on Perfect Gas Cases

- The nozzle exit pressure to freestream post-shock stagnation pressure ratio is of order unity
- 80% throttle leads to underexpanded nozzles
- 60% throttle leads to overexpanded nozzles
- Underexpanded nozzles lead to reduced pressure recovery on the vehicle, although have higher thrust and thus larger overall deceleration
- Overexpanded nozzles do lead to pressure recovery on the vehicle, although at the cost of less engine thrust
- One purpose of this study is to determine the forces and moments on the vehicle to determine the overall impact on guidance, stability, and control

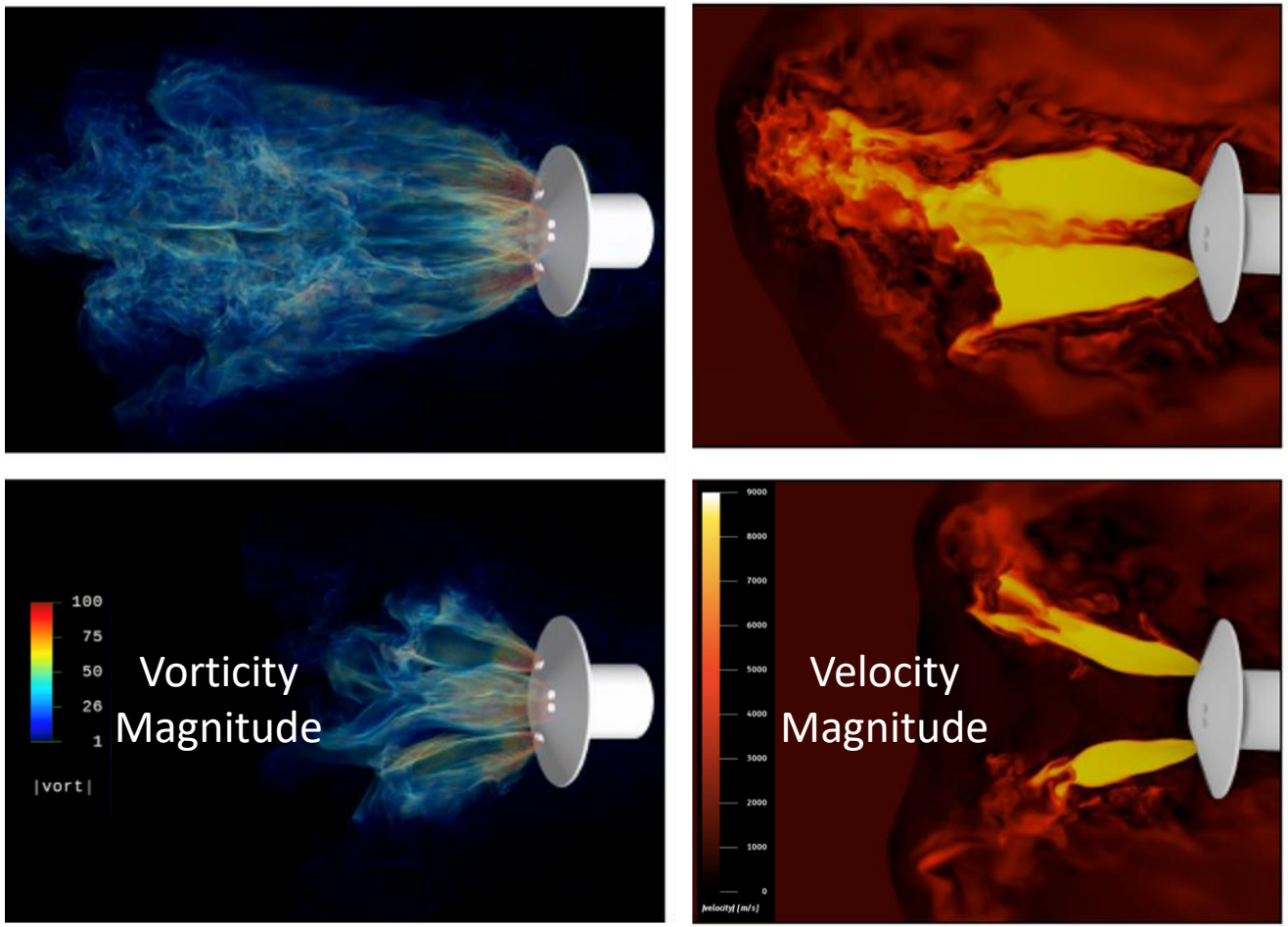

Visualization of perfect gas simulations for 511M point grid. Left: Instantaneous volume renderings of vorticity magnitude. Right: Instantaneous velocity magnitude contours. Top figures correspond to underexpanded nozzle condition (80% throttle). Bottom figures correspond to overexpanded nozzle condition (60% throttle).

Effect of Throttling on Chemistry Cases

Instantaneous Mean

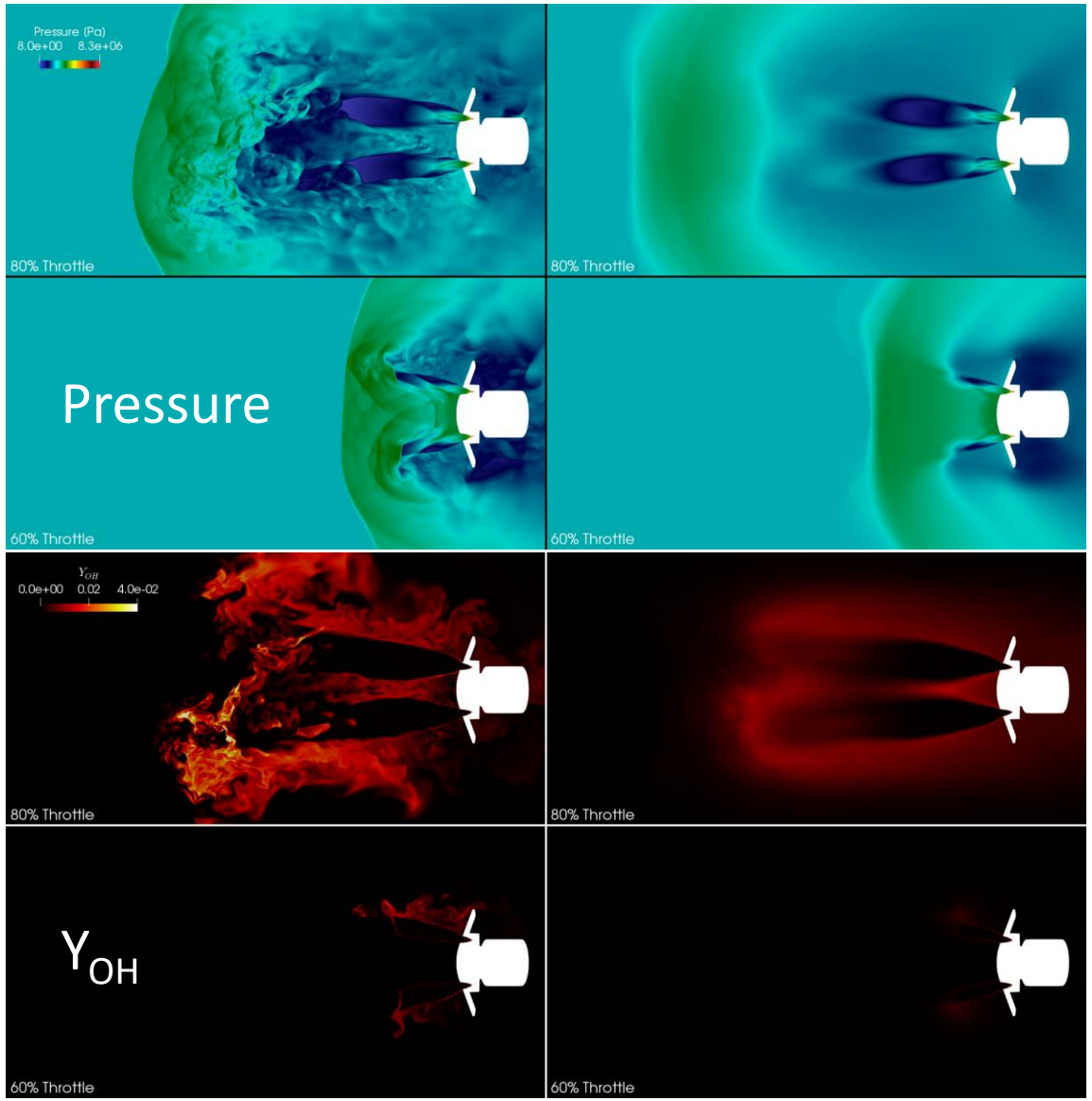

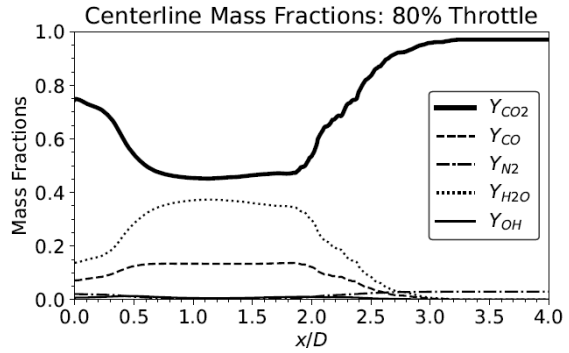

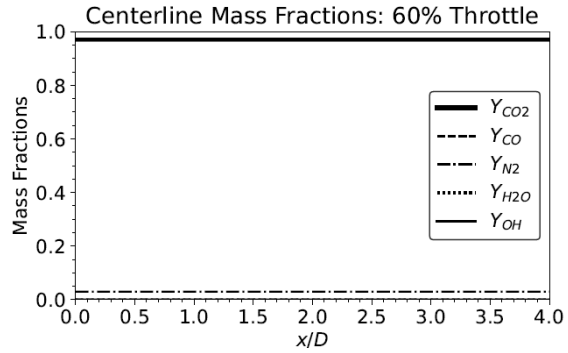

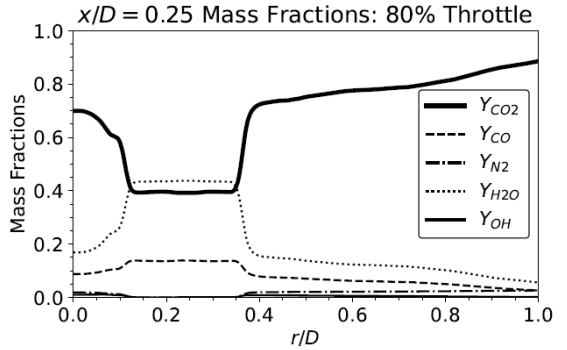

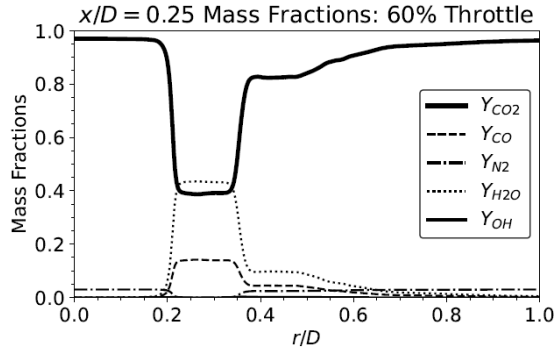

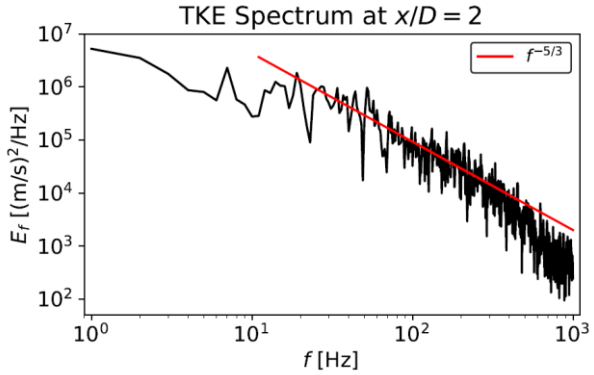

Force and Moment Comparisons

80% Throttle

Total Vehicle Aerodynamic Coefficients

	C_A		C_{ref}		$C_{m,ref}$	
Case	μ	σ	μ	σ	μ	σ
Perfect Gas 143M	0.0662	0.0415	-0.0002	0.0075	0.0003	0.0063
Perfect Gas 1.14B	0.0492	0.0512	0.0122	0.0066	-0.0152	0.0057
Reacting Gas 139M	0.0864	0.0536	0.0102	0.0102	0.0114	0.0094
Reacting Gas 1.11B	0.0912	0.0433	0.0084	0.0107	0.0093	0.0101

60% Throttle

Total Vehicle Aerodynamic Coefficients

	C_A	
Case	μ	σ
Perfect Gas 143M	0.3540	0.0337
Perfect Gas 1.14B	0.2865	0.0501
Reacting Gas 139M	0.4538	0.0232
Reacting Gas 1.11B	0.3999	0.0353

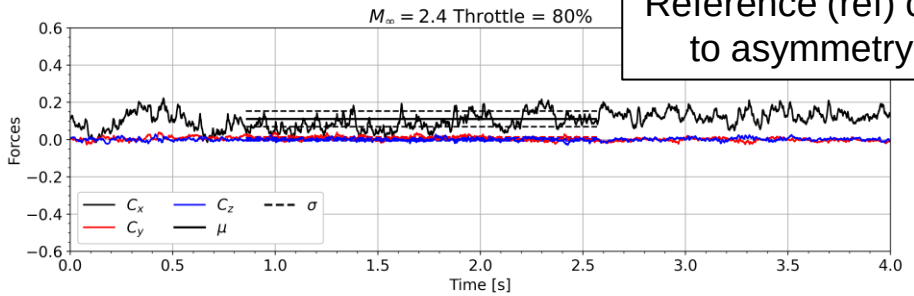

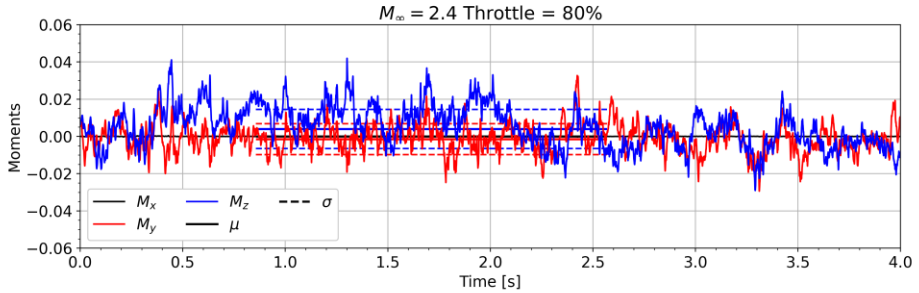

Reference (ref) corresponds to asymmetry direction

Pressure Coefficient

80% Throttle

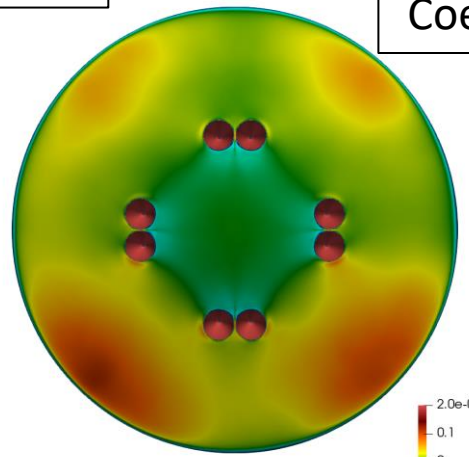

60% Throttle

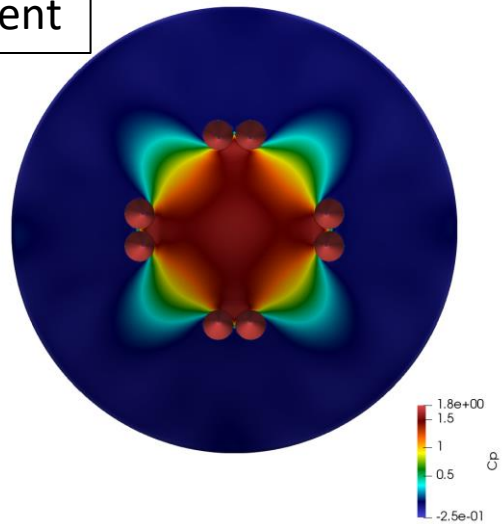

Total Axial Coefficient Breakdown

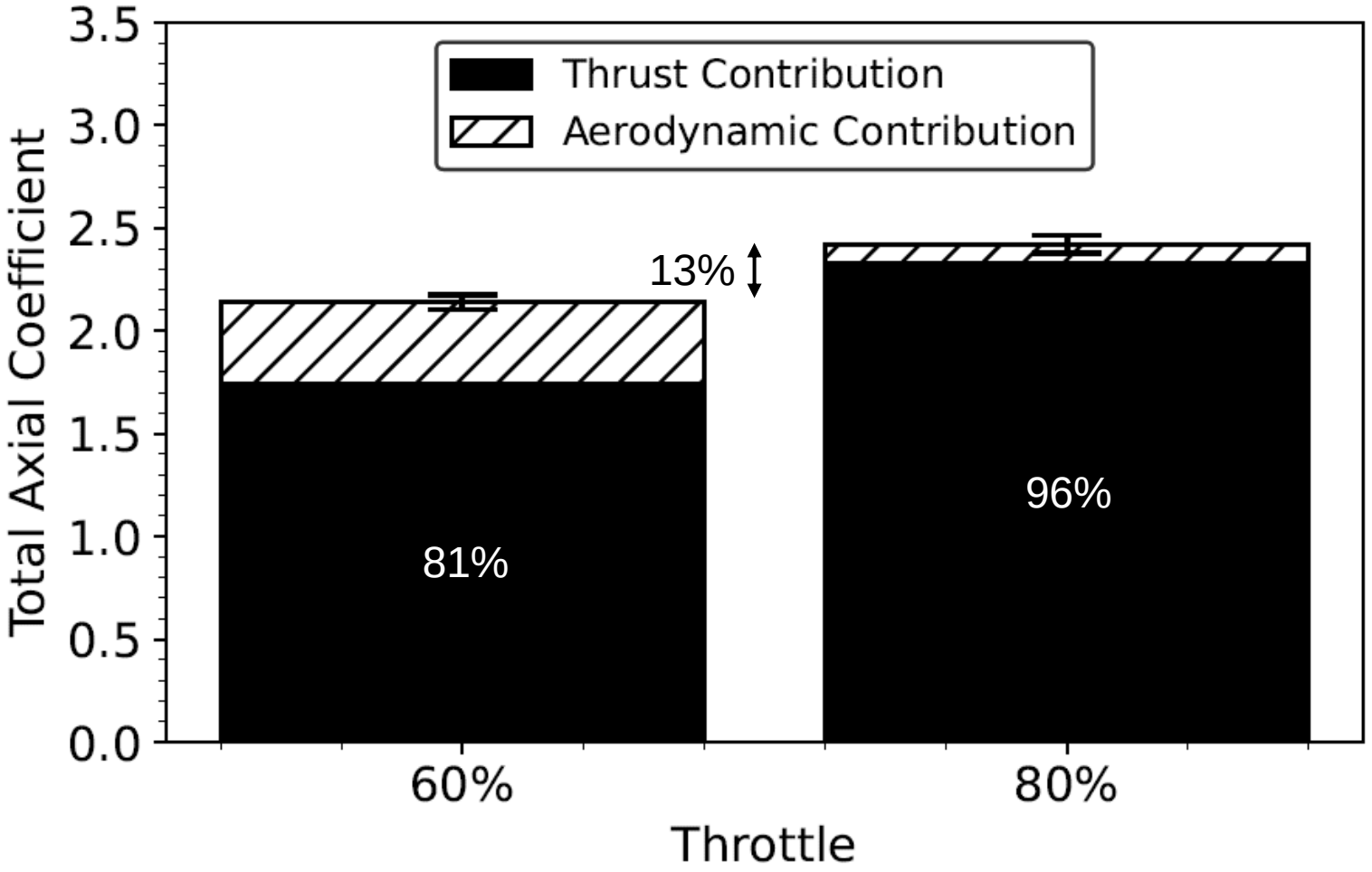

$$\sigma \approx 0.02\mu$$

Summary and Future Work

- Chemically reacting, scale-resolving supersonic retropropulsion simulations have been carried out for a human-scale Mars lander concept
- Flow structures are qualitatively similar to previous perfect gas air simulations
- Overall, the thrust accounts for the majority of the axial force on the vehicle
- Effects of gas chemistry versus perfect gas air include:
  - Significant minor species concentrations are present upstream of the vehicle for the 80% throttle cases
  - Specific heat ratio varies substantially in the nozzles and upstream of the vehicle due to strong temperature dependence of carbon dioxide and chemistry
  - For overexpanded plumes, reacting gas simulations predict 40% larger axial aerodynamic force compared to perfect gas air
  - For underexpanded plumes, reacting gas simulations predict 80% larger axial aerodynamic force compared to perfect gas air
- Future computational efforts should investigate inert pseudospecies with temperature dependent thermodynamic properties
- Future experimental efforts should examine the effects of chemistry on model problems representative of future Mars lander concepts for simulation validation